J|A|C|S
ARTICLES
Published on Web 07/20/2006

Microporous Metal−Organic Frameworks Formed in a Stepwise Manner from Luminescent Building Blocks

Brett D. Chandler, David T. Cramb,* and George K. H. Shimizu*

Contribution from the Department of Chemistry, University of Calgary, Calgary, Alberta, T2N 1N4, Canada

Received January 27, 2006; E-mail: dcramb@ucalgary.ca; gshimizu@ucalgary.ca

Abstract: A series of trivalent lanthanides (Sm, Eu, Gd, Tb, Dy) have been complexed to the dianionic ligand, 4,4′-disulfo-2,2′-bipyridine-*N,N*′-dioxide, L, in a 3:1 ratio to form trianionic complex building blocks. These units were then cross-linked into a network solid by addition of $BaCl_2$ to form mixed-metal networks of formula $\{Ba_2(H_2O)_4[LnL_3(H_2O)_2](H_2O)_nCl\}_\infty$, Ln = Sm^{3+} (**1**), Eu^{3+} (**2**), Gd^{3+} (**3**), Tb^{3+} (**4**), Dy^{3+} (**5**). The networks were isostructural and contained open channels which readily absorbed and desorbed water accompanied by a spongelike shrinkage and expansion of the host. CO_2 sorption measurements confirmed microporosity giving a DR surface area of 718 m^2/gm and an average pore size of 6.4 Å. Ligand L sensitized all the lanthanide ions with the exception of Gd^{3+}. Studying the series of Ln complexes allowed the determination of the triplet state energy of L which is itself a new ligand for sensitization purposes. The luminescent properties of the lanthanide building blocks were retained in the porous network solid. From the luminescence data, it was possible to attribute the spongelike properties of the network to the Ba^{2+} coordination sphere rather than the Ln^{3+} center. Networks were characterized by X-ray crystallography, PXRD, DSC/TGA, water vapor and gas sorption, and luminescence spectroscopy.

Introduction

Lanthanide ions are widely employed as phosphors for photonic applications such as light-emitting diodes, tunable lasers, and optical storage.[1] There are several properties of lanthanides which lead to their utility as phosphors.[2] Primarily, the range at which different Ln ions emit spans a wide spectrum from infrared radiation to blue light. Facilitating the study of these compounds is the fact that the 4f orbitals, between which transitions of optical interest occur, are shielded from their environment by the 5s and 5p orbitals, leading to desired sharp emission lines. Finally, the coordination chemistry of Ln ions with suitable "antenna" ligands is well studied.[3] Antenna ligands are efficient absorbers of radiation that possess an excited-state capable of sensitizing the emission of the Ln ions. This is preferable to direct excitation of the Ln ion as the Ln ions themselves are not strong absorbers, thus resulting in weaker emission.

Particularly with respect to sensor development, it would be highly desirable to couple the properties of a phosphor with a porous architecture.[4] Porosity in a solid brings with it its own synthetic challenges as enthalpy will favor a dense material. As such, much of the research in forming porous solids with Ln ions has involved impregnating solids already known to be permanently porous, for example, exchanging Ln ions for intrachannel cations in zeolites.[5] Another approach has involved forming Ln silicates with the Ln ion as an integral component of a framework where strong bonding to oxide ligands can sustain three-dimensional open structures or layered solids.[6] In the case of exchanged zeolitic solids, the local environment of the Ln ion is not easily determined and may be variable. In the Ln silicate approach, solids formed are ordered but synthetic control over the immediate coordination environment, and hence the luminescence properties, of the Ln ion is difficult. Additionally, the Ln ions in these systems require direct excitation and therefore are not as strongly emitting. Some systems have been reported where Ln coordination complexes were exchanged into zeolites[7] as well as into larger pore systems.[8] None of these approaches has yet reached maturity, and there are ample opportunities for new materials.

(1) (a) Blasse, G.; Grabmaier, B. C. *Luminescent Materials*; Springer-Verlag: Berlin, 1997. (b) Justel, T.; Nikol, H.; Ronda, C. *Angew. Chem., Int. Ed.* **1998**, *37*, 3085.
(2) (a) De Sa, G. F.; Malta, O. L.; Donega, C. D.; Simas, A. M.; Longo, R. L.; Santa-Cruz, P. A. da Silva, E. F. *Coord. Chem. Rev.* **2000**, *196*, 165. (b) Bunzli, J. C. G.; Piguet, C. *Chem. Soc. Rev.* **2005**, *34*, 1048.
(3) Whan, R. E.; Crosby, G. A. *J. Mol. Spectrosc.* **1962**, *8*, 315.
(4) (a) Rocha, J.; Carlos, L. D. *Curr. Opin. Solid State Mater. Sci.* **2003**, *7*, 1999. (b) Scott, B. J.; Wirnsberger, G.; Stucky, G. D. *Chem. Mater.* **2001**, *13*, 3140.
(5) (a) Suib, S. L.; Zerger, R. P.; Stucky, G. D.; Morrison, T. I.; Shenoy, G. K. *J. Phys. Chem.* **1984**, *80*, 2203. (b) Baker, M. D.; Olken, M. M.; Ozin, G. A. *J. Am. Chem. Soc.* **1988**, *110*, 5709. (c) Maas, H.; Curao, A.; Calferri, G. *Angew. Chem., Int. Ed.* **2002**, *41*, 2495.
(6) (a) Anianas, D.; Ferreira, A.; Rocha, J.; Ferreira, P.; Rainho, J. P.; Morais, C.; Carlos, L. D. *J. Am. Chem. Soc.* **2001**, *123*, 5735. (b) Rainho, J. P.; Pillinger, M.; Carlos, L. D.; Ribeiro, J. L.; Almeida, R. M.; Rocha, J. *J. Mater. Chem.* **2002**, *12*, 1162.
(7) (a) Wada, Y.; Okubo, T.; Ryo, M.; Nakazawa, T.; Hasegawa, Y.; Yanegida, S. *J. Am. Chem. Soc.* **2000**, *122*, 8583. (b) Sendor, D.; Kynast, U. *Adv. Mater.* **2002**, *14*, 1570.
(8) (a) Carlos, L. D.; Messadeq, Y.; Brito, H. F.; Fereira, R. A. S.; Bermudez, V. D.; Ribeiro, S. J. L. *Adv. Mater.* **2000**, *12*, 594. (b) Embert, F.; Mehdi, A.; Reye, C.; Corriu, R. J. P. *Chem. Mater.* **2001**, *13*, 4542. (c) Klonkowski, A. M.; Lis, S.; Pietraszkiewicz, M.; Hnatejko, Z.; Czarnobaj, K.; Elbanowski, M. *Chem. Mater.* **2003**, *15*, 656. (d) Guo, X. M.; Fu, L. S.; Zhang, H. J.; Carlos, L. D.; Peng, C. Y.; Guo, J. F.; Yu, J. B.; Deng, R. P.; Sun, L. N. *New. J. Chem.* **2005**, *29*, 1351.

The domain of metal−organic frameworks (MOFs) has seen several examples of Ln-containing solids reported.[9−16] The challenge of forming permanently porous materials is apparent with these compounds as the Ln coordination spheres are notoriously variable with respect to both coordination number and geometry.[9] In principle, this should result in more facile routes to densely packed solids. Indeed, relative to transition metals, the number of reported Ln MOFs with open structures is relatively small. The presence of solvent-filled pores in a structure is itself not necessarily evidence of porosity as many coordination polymer solids collapse upon solvent removal. Of the open framework Ln-containing MOFs reported, some report retention of structure with heating[10] and others report reversible solvent exchange.[11] Only a handful report characterization of porosity by gas sorption analyses.[12−14] Targeting porosity and luminescence in an MOF further restricts the choice of building blocks as, in addition to being able to sustain porosity, the ligand should act as an antenna to sensitize the Ln ion. Numerous Ln network solids with interesting luminescent properties, but with structures that are either dense or which do not retain porosity, have been reported.[15] Thus, the principal challenges facing a porous luminescent solid are to first generate porosity and then to have some element of predictability with respect to the luminescence of the solid stemming from the Ln coordination environment.

Herein we present an isostructural series of Ln-containing MOFs,[16] which couple porosity and luminescence, owing to their formation by a stepwise assembly approach. Cross-linkable derivatives of Ln coordination complexes of known luminescent properties were prepared and linked by addition of a second, nonluminescent metal center into three-dimensional solids with open channels. Upon solvent removal, the structures contracted but the new solids formed were microporous as demonstrated by both reversible CO_2 and water vapor sorption. Notably, the stepwise assembly enabled the luminescent properties of the building block complex to be retained in the framework solid. All the Ln ions with the exception of Gd were sensitized by the antenna ligand, and we report the triplet state energy of the ligand. Luminescence lifetimes were found to vary with hydration and other guests in the channels of the solid. Assessing the symmetry of the Ln ions indicated that the geometry of the centers was consistent in the solvated and desolvated forms which allows us to attribute the structural dynamics of the network to the secondary cross-linking interactions. The results show the promise of metal complexes as nodes in metal−organic frameworks both for their ability to sustain permanent porosity and for their ability to incorporate physicochemical functions.

Experimental Section

The synthesis of 4,4′-disulfo-2,2′-bipyridine *N*,*N*′-dioxide, L, was prepared as described elsewhere.[17] The synthesis of each compound proceeded via a stepwise approach. $LnCl_3$ (Ln = Sm, Eu, Gd, Tb, Dy) was complexed with H_2L in water to generate in situ $[LnL_3(H_2O)_2]^{3-}$. This anionic species was then complexed with $BaCl_2$ in aqueous solution to form the complex $\{Ba_2(H_2O)_4[LnL_3(H_2O)_2](H_2O)_nCl\}_\infty$, Ln = Sm, **1**; Eu, **2**; Gd, **3**; Tb, **4**; Dy, **5**. Crystals were obtained from vapor diffusion of acetone into water. Details of the preparation and full characterization are provided as Supporting Information.

Single-crystal diffraction experiments were conducted at 173 K for structures **2**−**5**; **1** was collected at 193 K. All samples were collected using a Nonius Kappa CCD diffractometer with graphite monochromated Mo Kα radiation (λ = 0.710 69 Å) and equipped with a CCD detector. The intensity data collection was performed in the $\omega-\phi$ scanning mode with the goniometer and detector angular settings optimized using the program COLLECT.[18] The crystal-to-detector distance was 30 mm. The unit cell and the orientation matrix were refined using the entire data set of reflections. The diffraction spots were measured in full with a high accuracy, scaled with SCALEPACK,[18] corrected for Lorentz-polarization correction, and integrated using DENZO.[18] The crystallographic data and conditions for structure analysis are listed in Table 1. Structure solutions (SIR97)[19] and refinements (SHELXL-97)[20] were run in the space groups $P2_1/c$ for all structures. The structure model (non-hydrogen atoms) was readily obtained from successive difference Fourier maps. All aromatic hydrogen atoms were placed using AFIX 43, and the remaining hydrogen atoms on the water molecules were not placed due to the disorder observed. At the end of refinement, anisotropic displacement parameters and extinction coefficients were allowed to vary, with the resulting residuals listed in Table 1.

Thermogravimetric analyses (TGA) were carried out in a nitrogen atmosphere in a Netzsch STA449C Jupiter analyzer using heating and cooling rates of 5 K/min. Vapor sorption experiments were performed on the TGA as follows. Samples were heated for 3 h at 160 °C until desolvation was complete and cooled to room temperature for 1.5 h. Guest uptake experiments were performed by passing a stream of nitrogen over a guest solvent at a flow rate of 40 mL/min for 2 h at 25 °C and passing this gas into the sample chamber. Finally, the sample was purged with dry nitrogen for an additional 2 h to remove any surface adsorbed guest and reach full equilibration at 25 °C. The newly solvated samples were then desolvated as previously described. CO_2 sorption measurements were performed at Quantachrome Instruments on an Autosorb 1 Surface Area and Pore Size Analyzer at 0 °C after outgassing at 200 °C for 5 h and using a cross-sectional area of 21 Å^2 for CO_2. Room-temperature phosphorescence measurements and lifetime determinations were carried out using a Varian Cary Eclipse fluorescence spectrophotometer with excitation and emission slit widths of 2.5 nm spectral resolution. Lifetime data collection proceeded using a single flash with a delay of 100 μs, a gate time of 500 μs, and a decay of 5 ms unless otherwise noted. Lifetime data were fit using a

(9) Hill, R. J.; Long, D.; Hubberstey, P.; Schröder, M.; Champness, N. R. *J. Solid State Chem.* **2005**, *178*, 2414.
(10) (a) Millange, F.; Serre, C.; Marrot, J.; Gardant, N.; Pellé, F.; Férey, G. *J. Mater. Chem.* **2004**, *14*, 642. (b) Dimos, A.; Tsaousis, D.; Michaelides, A.; Skoulika, S.; Golhen, S.; Ouahab, L.; Didierjean, C.; Aubry, A. *Chem. Mater.* **2002**, *14*, 2616. (c) Chen, X.-Y.; Zhao, B.; Shi, W.; Xia, J.; Cheng, P.; Liao, D.-Z.; Yan, S.-P.; Jiang, Z.-H. *Chem. Mater.* **2005**, *17*, 2866.
(11) (a) Reineke, T. M.; Eddaoudi, M.; Fehr, M.; Kelley, D.; Yaghi, O. M. *J. Am. Chem. Soc.* **1999**, *121*, 1651. (b) Maji, T. K.; Mostafa, G.; Chang, H.-C.; Kitagawa, S. *Chem. Commun.* **2005**, 2436. (c) Serpaggi, F.; Férey, G. *J. Mater. Chem.* **1998**, *8*, 2737. (d) Serpaggi, F.; Luxbacher, T.; Cheetham, A. K.; Férey, G. *J. Solid State Chem.* **1999**, *145*, 580.
(12) (a) Reineke, T. M.; Eddaoudi, M.; O'Keeffe, M.; Yaghi, O. M. *Angew. Chem., Int. Ed.* **1999**, *38*, 2590. (b) Rosi, N. L.; Kim, J.; Eddaoudi, M.; Chen, B.; O'Keeffe, M.; Yaghi, O. M. *J. Am. Chem. Soc.* **2005**, *127*, 1504.
(13) Pan, L.; Adams, K. M.; Hernandez, H. E.; Wang, X.; Zheng, C.; Hattori, Y.; Kaneko, K. *J. Am. Chem. Soc.* **2003**, *125*, 3062.
(14) Devic, T.; Serre, C.; Audebrand, N.; Marrot, J.; Férey, G. *J. Am. Chem. Soc.* **2005**, *127*, 12788.
(15) (a) Ma, L.; Evans, O. R.; Foxman, B. M.; Lin, W. B. *Inorg. Chem.* **1999**, *38*, 5837. (b) Serpaggi, F.; Férey, G.; Antic-Fidancev, E. *J. Solid State Chem.* **1999**, *148*, 347. (c) Serre, C.; Pelle, F.; Gardant, N.; Férey, G. *Chem. Mater.* **2004**, *16*, 1177. (d) Serre, C.; Millange, F.; Thouvenot, C.; Gardant, N.; Pellé, F.; Férey, G. *J. Mater. Chem.* **2004**, *14*, 1540. (e) De Lill, D. T.; Gunning, N. S.; Cahill, C. L. *Inorg. Chem.* **2005**, *44*, 258. (f) Kim, Y.; Suh, M.; Jung, D.-Y. *Inorg. Chem.* **2004**, *43*, 245.
(16) The structure of one member of this series and a vapor sorption study were reported in a preliminary communication, Chandler, B. D.; Côté, A. P.; Cramb, D. T.; Hill, J. M.; Shimizu, G. K. H. *Chem. Commun.* **2002**, 1900.
(17) Anderson, S.; Constable, E. C.; Seddon, K. R.; Turp, J. E. *J. Chem. Soc., Dalton Trans.* **1985**, 2247.
(18) COLLECT, DENZO, SCALEPACK, SORTAV, Kappa CCD Program Package; Nonius BV: Delft, The Netherlands, 1998.
(19) Altomare, A.; Burla, M. C.; Camalli, M.; Cascarano, G. L.; Giacovazzo, C.; Guagliardi, A.; Moliterni, A. G. G.; Polidori, G.; Spagna, R. *J. Appl. Crystallogr.* **1999**, *32*, 115.
(20) Sheldrick. G. M. *SHELXL-97, Program for crystal structure refinement*; University of Göttingen: Germany, 1997.

Table 1. Summary of Crystallographic Data for Compounds **1**, **2**, **4**, and **5**

	1	2	3	4	5
formula	$C_{30}H_{18}Ba_2ClN_6O_{37.14}S_6Sm$	$C_{30}H_{18}Ba_2ClN_6O_{35.44}S_6Eu$	$C_{30}H_{18}Ba_2ClN_6O_{39.16}S_6Gd$	$C_{30}H_{18}Ba_2ClN_6O_{38.22}S_6Tb$	$C_{30}H_{18}Ba_2ClDyN_6O_{34.48}S_6$
fw	1709.64	1683.98	1748.62	1743.91	1679.22
space group	$P2_1/c$	$P2_1/c$	$P2_1/c$	$P2_1/c$	$P2_1/c$
a, Å	24.579(5)	24.550(2)	24.423(5)	24.525(5)	24.627(5)
b, Å	23.016(5)	23.026(2)	22.995(5)	22.917(5)	22.651(5)
c, Å	10.511(5)	10.4867(10)	10.498(2)	10.531(5)	10.547(5)
α, deg	90	90	90	90	90
β, deg	98.64(4)	98.8(1)	98.54(3)	98.6(1)	98.17(4)
γ, deg	90	90	90	90	90
V, Å^3	5878.66(3)	5858.5(10)	5830.0(2)	5852.37(3)	5823.71(3)
Z	4	4	4	4	4
T, K	173(2)	193(2)	173(2)	173(2)	173(2)
λ, Å	0.710 69	0.710 73	0.710 69	0.710 69	0.710 69
d_{calcd}, g cm^{-3}	1.938	1.899	1.994	1.979	1.911
μ, mm^{-1}	2.672	2.741	2.828	2.891	2.964
F(000)	3308	3270	3372	3360	3220
R^a	0.0471	0.0614	0.0480	0.0585	0.0379
$R_w{}^b$	0.0775	0.0920	0.1341	0.1253	0.0650

[a] $R = [\sum||F_o| - |F_c||]/[\sum|F_o|]$ for reflections with $I > 2.00\sigma(I)$. [b] $R_w = \{[\sum w(F_o^2 - F_c^2)^2]/[\sum w(F_o^2)^2]\}^{1/2}$ for all reflections.

Scheme 1. Stepwise, Building Block Approach to Microporous Ln Solids Employed in This Work

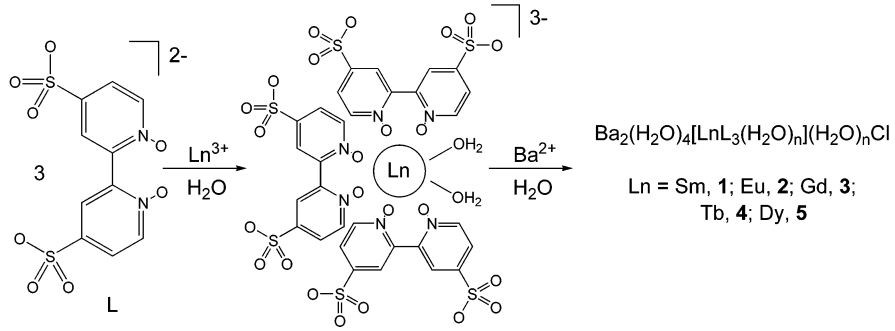

first-order single exponential with a good quality of fit based on the reduced chi-square statistics. Low-temperature phosphorescence measurements were performed with an Edinburgh Instruments FS/FL instrument with a 450 W Xe arc lamp. The excitation light was fed to a monochromator (single grating, 1800 lines/mm) and focused on a square quartz cuvette (1×1 cm^2) containing a glycerol−water mixture (5 parts glycerol and 4 parts 0.05 M borate buffer, pH 9.2) cooled to 77 K with liquid nitrogen. The emitted visible light was fed to a second monochromator (1800 lines/mm grating) and collected on a red-sensitive Peltier element cooled Hamamatsu R955 photomultiplier tube.

Results and Discussion

Stepwise Assembly Approach. A stepwise approach to the formation of metal−organic frameworks, depicted in Scheme 1, has been employed in this work for two reasons. First was to permit the incorporation of a lanthanide center with a defined coordination environment and hence a predictable fluorescent center into a framework. The second reason was structural in that a metal complex as a building block could impart enhanced stability to the solid in the sense that it is a "clusterlike" node as well as providing greater control over network formation. Lanthanide ions, particularly Eu(III), are known to be efficiently sensitized by chelation to 2,2′-bipyridine-*N*,*N*′-dioxide to a maximum stoichiometry of 4:1 L:M.[21] To employ a stepwise approach requires the incorporation of a secondary coordination site. As such, the ligand, 4,4′-disulfo-2,2′-bipyridine *N*,*N*′-dioxide, L, was prepared.[17] The sulfonate groups represent the second binding site, and we[22] and others[23,24] have been exploring the network-forming potential of this functionality. Heavier alkaline earth ions with sulfonate ions have been shown to be promising for the formation of robust metal−organic frameworks,[25] and in this work, Ba^{2+} was employed as the cross-

(21) Huskowska, E.; Riehl, J. P. *J. Lumin.* **2000**, *86*, 137.

(22) (a) Côté, A. P.; Shimizu, G. K. H. *Coord. Chem. Rev.* **2003**, *245*, 49. (b) Mäkinen, S. K.; Melcer, N. J.; Parvez, M.; Shimizu, G. K. H. *Chem.—Eur. J.* **2001**, *7*, 5176. (c) May, L. J.; Shimizu, G. K. H. *Chem. Mater.* **2005**, *17*, 217. (d) Hoffart, D. J.; Dalrymple, S. A.; Shimizu, G. K. H. *Inorg. Chem.* **2005**, *44*, 8868. (e) Côté, A. P.; Shimizu, G. K. H. *Inorg. Chem.* **2004**, *43*, 6663. (f) Côté, A. P.; Ferguson, M. J.; Khan, K. A.; Enright, G. D.; Kulynych, A. D.; Dalrymple, S. A.; Shimizu, G. K. H. *Inorg. Chem.* **2002**, *41*, 287.

(23) (a) Cai, J. W. *Coord. Chem. Rev.* **2004**, *248*, 1061. (b) Atwood, J. L.; Barbour, L. J.; Hardie, M. J.; Raston, C. L. *Coord. Chem. Rev.* **2001**, *222*, 3.

(24) (a) Chen, C. H.; Cai, J. W.; Liao, C. Z.; Feng, X. L.; Chen, X. M.; Ng, S. W. *Inorg. Chem.* **2002**, *41*, 4967. (b) Li, F. F.; Ma, J. J.; Song, S. Y.; Yang, J.; Liu, Y. Y.; Su, Z. M. *Inorg. Chem.* **2005**, *44*, 9374. (c) Cai, J. W.; Zhou, J. S.; Lin, M. L. *J. Mater. Chem.* **2003**, *13*, 1806. (d) Sun, D. F.; Cao, R.; Bi, W. H.; Li, X. J.; Wang, Y. Q.; Hong, M. C. *Eur. J. Inorg. Chem.* **2004**, *10*, 2144. (e) Kennedy, A. R.; Hughes, M. P.; Monaghan, M. L.; Staunton, E.; Teat, S. J.; Smith, W. E. *J. Chem. Soc., Dalton Trans.* **2001**, 2199. (f) Cai, J. W.; Chen, C. H.; Feng, X. L.; Liao, C. Z.; Chen, X. M. *J. Chem. Soc., Dalton Trans.* **2001**, 2370. (g) Liu, Y.; Su, J.; Li, W.; Wu, J. *Inorg. Chem.* **2005**, *44*, 3890. (h) Mezei, G.; Raptis, R. G. *New J. Chem.* **2003**, *27*, 1399. (h) Park, S. H.; Lee, C. E. *Chem. Commun.* **2003**, 1838. (i) Chandrasekhar, V.; Boomishankar, R.; Singh, S.; Steiner, A.; Zacchini, S. *Organometallics* **2002**, *21*, 4575. (j) Kennedy, A. R.; Kirkhouse, J. B. A.; McCarney, K. M.; Puissegur, O.; Smith, W. E.; Staunton, E.; Teat, S. J.; Cherryman, J. C.; James, R. *Chem.—Eur. J.* **2004**, *10*, 4606. (k) Sun, Z. M.; Mao, J. G.; Sun, Y. Q.; Zeng, H. Y.; Clearfield, A. *Inorg. Chem.* **2004**, *43*, 336. (l) Ma, J. F.; Yang, J.; Li, S. L.; Song, S. Y.; Zhang, H. J.; Wang, H. S.; Yang, K. Y. *Cryst. Growth Des.* **2005**, *5*, 807.

(25) (a) Dalrymple, S. A.; Shimizu, G. K. H. *Chem.—Eur. J.* **2002**, *8*, 3010. (b) Côté, A. P.; Shimizu, G. K. H. *Chem.—Eur. J.* **2003**, *9*, 5361. (c) Liu, Y. F.; Su, J. C.; Li, W. H.; Wu, J. G. *Inorg. Chem.* **2005**, *44*, 3890. (d) Côté, A. P.; Shimizu, G. K. H. *Chem. Commun.* **2002**, 251. (e) Hoffart, D. J.; Côté, A. P.; Shimizu, G. K. H. *Inorg. Chem.* **2003**, *42*, 8603.

linking ion. Formation of a 4:1 L:M complex would result in building blocks of the form $[ML_4]^{5-}$ where the metal center would be expected to adopt a square antiprismatic geometry based upon the nonsulfonated analogues. Importantly, no two monoanionic sulfonate groups on the same molecule of L are in sufficient proximity so as to be able to ligate to a single dicationic barium center, and so there will be a natural tendency toward an aggregated species. Only a handful of examples exist where a stepwise approach has been employed toward the synthesis of a metal−organic framework. Systems employing derivatives of acac[26] and dipyrrin[27] ligands have been reported, but to our knowledge, this is the only example involving a Ln and where the building block has been selected for its physicochemical properties.

Complexes of the type $[ML_4]^{5-}$ as their Na salts were prepared and then cross-linked with the heavier alkaline earth ions. However, a single-crystal X-ray determination of a Sr^{2+} cross-linked structure revealed that, while a robust structure of cross-linked building blocks was obtained, the 4-fold symmetry, and roughly spherical nature of the $[ML_4]^{5-}$ complexes enabled the facile formation of a dense, nonporous structure.[28] While a dense solid was not desired, this provided an opportunity to show an advantage of a stepwise synthetic approach. Changing the stoichiometry of the building block preparation to 3:1 L:M resulted in the formation of complexes of formula $[ML_3(H_2O)_2]^{3-}$. Cross-linking of these units with Ba^{2+} resulted in the formation of solids where the absence of the fourth chelating molecule of L on each lanthanide center serves to enable pores to form. This microporous family of compounds and their luminescence properties are the subject of the present work. As the solids are isostructural, differing only slightly by hydration and a slight contraction of the Ln coordination sphere as expected, details will only be provided for the Eu analogue, **2**.

Structural Description. In a typical preparation, $EuCl_3$ was complexed with H_2L in water to generate the soluble species $H_3[EuL_3(H_2O)_2]$. This compound was complexed with $BaCl_2$ in an aqueous solution to form the complex, $Ba_2(H_2O)_4[EuL_3(H_2O)_2](H_2O)_{5.44}Cl$, **2**. Single crystals were obtained via diffusion of acetone into an aqueous solution of **2**. Compound **2** forms a three-dimensional framework consisting of $[EuL_3(H_2O)_2]^{3-}$ units cross-linked by Ba^{2+}−sulfonate interactions (Figure 1). In **2**, the asymmetric unit (Figure 2) is composed of one Eu^{3+} center, three molecules of L, two Ba^{2+} ions, one Cl^- ion, and three types of water molecules, that is, those bound to Ba, those bound to Eu, and those uncoordinated in the channels. The structure contains channels that run along the *c*-axis. The dimensions of these channels are approximately 12.49 Å high with a width of 9.84 Å as defined by the shortest trans-channel metal−metal distances. These values convert to ~8.5 × 5.8 Å^2 when van der Waals radii are considered. This reference was chosen owing to the labile nature of the aquo ligands on both Ba and Eu centers and the fact these sites point directly into the channels. Uncoordinated disordered water molecules, ~5.5 per Eu center as modeled crystallographically, occupy the channels. The shortest trans-channel distances between aquo ligands are 8.41 and 5.34 Å. The full coordination sphere of the Eu center is composed of six oxygen atoms from the *N*-oxides of three molecules of L and two aquo ligands directed into the channel. There is no coordination of sulfonate oxygen atoms to the Ln center.

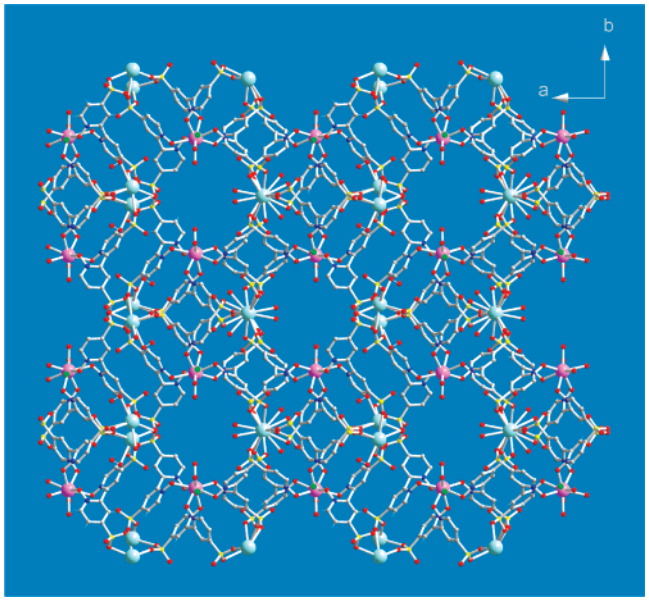

Figure 1. Single-crystal structure of the Eu complex, **2**, showing the one-dimensional pores that permeate the solid. Color scheme: Eu, pink; Ba, gray (large); S, yellow; O, red; C, gray (small).

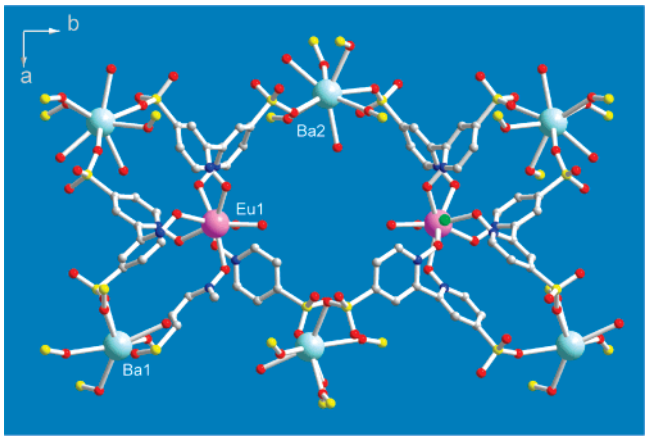

Figure 2. View of a single channel in **2**. Each pore is lined by two of the triply chelated Ln building blocks. The coordination spheres of the Ba ions are completed, and sulfonate oxygen atoms are depicted with their S atom shown to illustrate the extensive cross-linking. Note also the Cl^- situated in front of the Eu center on the right.

The interactions between the sulfonate groups and the alkaline earth ions serve to form a highly aggregated structure as one Ba center cross-links four of the $[EuL_3(H_2O)_2]^{3-}$ building blocks and the other Ba center links five such units. Ba1 is nine-coordinate with an irregular coordination sphere comprised of seven sulfonate oxygen atoms, from six different sulfonate groups, and two water molecules. These six sulfonate groups originate from six different molecules of L which in turn are associated with four different $[EuL_3(H_2O)_2]^{3-}$ building blocks. The coordination environment about Ba_2 is a distorted square antiprism of two water molecules and six sulfonate oxygen atoms. The six sulfonate oxygen atoms are again from six different sulfonate groups associated with six different molecules

(26) The systems in refs 26 and 27 result in controlled formation of heterometallic assemblies, but as of yet, none of the structures reports gas sorption. Chen, B. L.; Fronczek, F. R.; Maverick, A. W. *Inorg. Chem.* **2004**, *43*, 8209.
(27) (a) Halper, S. R.; Cohen, S. M. *Inorg. Chem.* **2005**, *44*, 486. (b) Murphy, D. L.; Malachowski, M. R.; Campana, C. F.; Cohen, S. M. *Chem. Commun.* **2005**, 5506.
(28) Chandler, B. D.; Shimizu, G. K. H. Unpublished results.

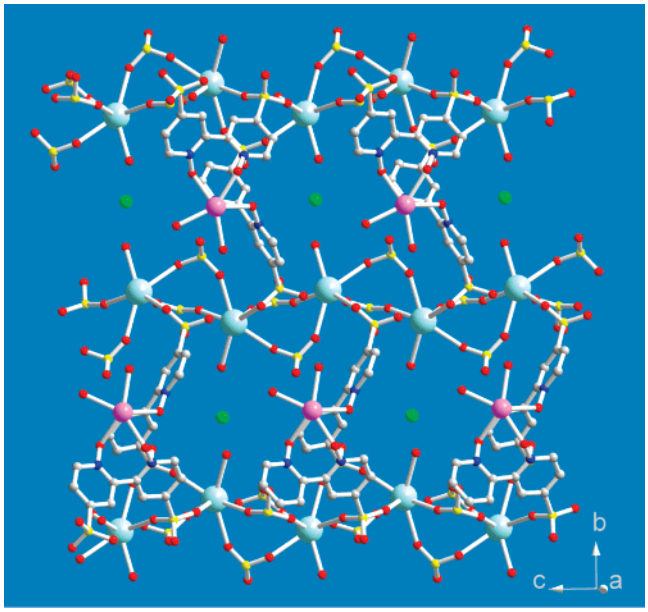

Figure 3. View approximately down the *a*-axis in **2** showing the formation of one-dimensional columns of SO_3-bridged Ba ions. The columns link the Eu building blocks into a 3-D network. The green spheres depict the inexchangeable Cl^- ions which lie between Eu centers.

of L. In this case, the Ba^{2+} ions serve to bring together five $[EuL_3(H_2O)_2]^{3-}$ luminescent units. This extensive cross-linking in the framework is to be expected as stated earlier.

In compound **2**, as in each of **1**−**5**, chloride ions are included as part of the structure. As the 4:1 building block had formed a dense solid, the removal of one dianionic ligand from the building block necessitates in the inclusion of additional negative charge. There exist smaller dome-shaped cavities off the sides of the water-filled channels, behind the lanthanide centers, where the Cl^- ions reside. Each Cl^- ion forms H-bonds to one lanthanide-bound water molecule (O···Cl = 3.133 Å) and the protons of four different α-carbons of pyridine rings (Cl···C 3.60(1)−3.85(1) Å, Cl···H−C 166.2(3)°−178.8(3)°). Figure 3 shows the location of these highly H-bonded "grottos" relative to the channels depicted in Figure 1. In Figure 3, the channels lie in a horizontal fashion adjacent to the rows of Ba^{2+} ions. A relative positioning of the channel can be envisioned by the placement of the aquo ligands on the Eu center as they are pointed directly into the channels. Attempts to exchange the Cl^- ions were unsuccessful confirming the strong binding of the anions by the H-bonds.

Porosity. Given the openness of the structures, their stability and porosity were examined. Thermogravimetric analyses of **2** showed a steady mass loss to 105 °C corresponding to loss of both free and coordinated water molecules (13.29% obsd, 13.42% calcd). This sample was then stable to 320 °C. Powder X-ray diffraction measurements after dehydration showed the solid to be amorphous. Interestingly, single crystals of **2** allowed to dry still extinguished polarized light but would no longer diffract X-rays. The reversibility of the dehydration was examined by placing a sample of **2** on the TGA and heating to dehydration. This was followed by cooling and the introduction of water vapor. In 1 h, the dry sample resorbed 95% of the lost water and, notably, the solid regained order. This process was completely reversible as shown in Figure 4. If left for longer periods (days), even in the ambient atmosphere, dehydrated single crystals of **2** rehydrated such that the single crystal could be recollected with virtually identical cell parameters to the nascent solid.[29] It was important to note that the amorphous nature of the dehydrated solid did not require a complete collapse of the network to a dense phase. Indeed, given the 3-fold chelated building block, contraction to a dense phase seemed quite unlikely. The porosity of **2** was further examined by gas sorption measurements. Upon outgassing for 5 h at 200 °C, a CO_2 sorption isotherm, run at 273 K, confirmed a porous solid was indeed retained (Figure 5). A Dubinin−Radushkevich (DR) analysis gave a surface area of 718 m^2/g, an average pore width of 6.2 Å, and a micropore volume of 0.25 mL/g. The observed rapid onset of CO_2 sorption at very low pressures is characteristic of the presence of micropores in the solid. Thus, despite the formation of an amorphous solid upon dehydration, the dry phase of **2** possessed a high degree of porosity. Figure 5 also shows considerable hysteresis in the desorption curve. The observed value for the energy of adsorption for CO_2 of 21.0 kJ/mol is consistent with a physisorption process. A N_2 sorption isotherm, run at 77 K, with identical outgas conditions to the CO_2 analysis yielded a strikingly smaller surface area (15 m^2/gm). Similar behavior has been reported by Pan et al. for the Ln-based MOF, Er(1,4-phenylenediacetate),[13] which shows pronounced CO_2 sorption but nonporous behavior toward N_2 and Ar. The authors attribute this observation to a combination of stronger affinity of the CO_2 for the host solid and also a critical difference in kinetic diameters of the different sorbates relative to the pores in the host. In our case, the DR analysis clearly indicates the pore size in the solid (6.4 Å) is of sufficient size to permit both CO_2 (3.30 Å) and N_2 (3.64 Å) access to the structure. To further examine this, the CO_2 sorption experiment was repeated at −42 °C using a dry ice/acetonitrile bath and gave a DR surface area of 210 m^2/g. This result affirms that **2** has permanent pores accessible to CO_2. This result also does affirm that there is activation of the solid by CO_2 sorption as was inferred by the observed hysteresis on desorption. However, it would appear unlikely that the sorption of CO_2 is due exclusively to activation of the solid. This result is not that surprising given that, using the building block approach, collapse to a completely dense solid is difficult. As will be discussed in the luminescence section, the Ln center largely retains its nascent geometry.

The phenomenon of markedly different observed surface areas based on CO_2 or N_2 isotherms is not uncommon for a microporous material. This is due to a combination of factors ultimately leading to a high activation barrier for N_2 molecules to diffuse through the pores and the blocking of access to much of the internal surface. The major contributions to this effect are the presence of a narrow micropore, the lower temperature employed for the N_2 analysis, the slightly larger diameter of N_2 versus CO_2, and the topology of the pore structure. Regarding the last point, a 3-D pore network, such as those observed in MOF-5,[30] would still permit access to internal surfaces if one or multiple pore openings became blocked by condensed N_2 molecules. In the case of **2**, pores are one-dimensional and so problems with diffusion of N_2 are magnified. This observation

(29) Upon sitting in the ambient atmosphere for 3 weeks, a crystal was mounted and the following cell obtained: monoclinic, space group $P2_1/c$ (No. 14), a = 24.484(8) Å, b = 22.977(9) Å, c = 10.490(6) Å, $\alpha = \gamma = 90°$, β = 98.33(1)°.

(30) Li, H.; Eddaoudi, M.; O'Keeffe, M.; Yaghi, O. M. *Nature* **1999**, *402*, 276.

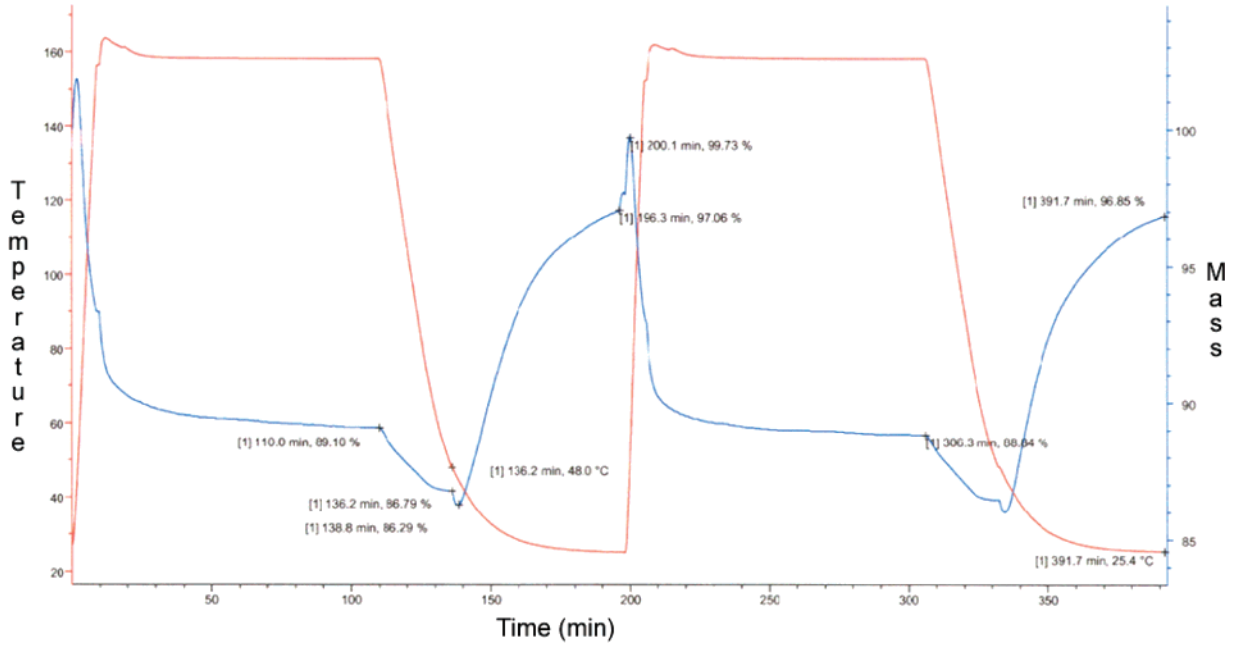

Figure 4. Reversible water vapor sorption by **2** as demonstrated on the TGA. The red curve represents the heating cycle employed to dehydrate the sample. This is accompanied by concurrent mass loss shown by the blue trace. Water vapor is then introduced, and the mass is seen to revert back close to the original value. A second cycle is then performed.

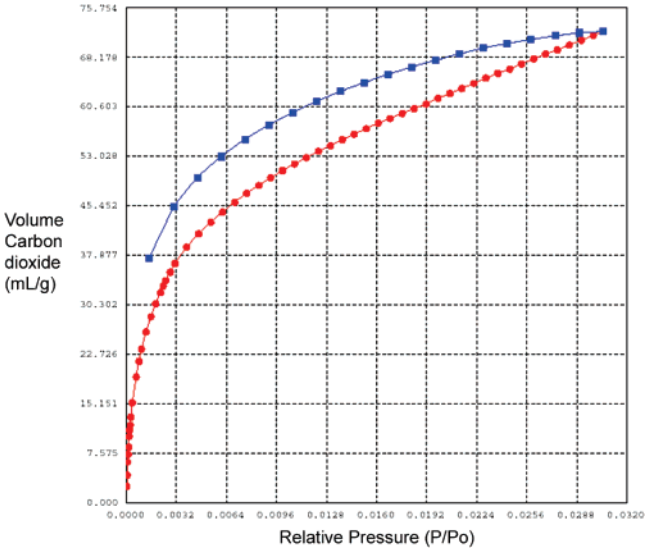

Figure 5. Carbon dioxide sorption isotherm for **2**, where the red line is adsorption and the blue line is desorption. A Dubinin−Radushkevich (DR) analysis gave a surface area of 718 m^2/g for **2** confirming microporosity.

has significant precedence in other families of microporous solids including activated carbons,[31] silicas,[32] cements,[33] and soils.[34]

For **2**, the values of 718 m^2/g as a microporous surface area and 0.25 mL/g as a micropore volume compare favorably to those of, for example, zeolite ZSM-5 for which the BET surface area and micropore volume are 431 m^2/g and 0.16 mL/g,[35] respectively. MOF structures have been reported with surface areas as high as 4500 m^2/g by Yaghi,[36] and 5900 m^2/g by Férey.[37] In comparison to other Ln-containing MOFs, the Férey group reported their MIL-103 had a Langmuir surface area from 1030 to 1330 m^2/g depending on the sample. [14]

Luminescence Studies. In addition to facilitating the formation of a porous solid, the other chief reason for employing the particular complex building block was to enable the incorporation of an efficient phosphor into such a solid. Due to the low molar absorptivity of the lanthanides, direct excitation produces weak emission spectra. Significantly enhanced emission can result when the metals are complexed or chelated to organic moieties that can efficiently absorb and transfer energy. Although numerous energy transfer mechanisms have been reported, the mechanism reported by Whan and Crosby[3] has to date been the most successful in explaining what is commonly referred to as the "antenna effect". This occurs from direct excitation of the ligand to a singlet state followed by an intersystem crossing to a triplet state. Successful emission from the metal results when a nonradiative energy transfer occurs from the ligand triplet state to the lanthanide ion. The newly excited lanthanide ion can then emit a photon or relax via a series of nonradiative processes.

The 2,2′-dipyridyl core used in the formation of complexes **1**−**5** absorbs strongly in the UV region and is an attractive ligand for sensitizing Eu, Dy, Sm, and Tb via the antenna effect. The ligand, L, is fluorescent at room temperature and exhibits a broad emission band over the blue-green region of the visible spectrum with a maximum appearing at 473 nm. The excitation spectrum shows two main peaks, 325 nm and 395 nm, with the lower energy transition being the most intense. The triplet state of L was determined from the 77 K phosphorescence spectrum obtained from the complexation with Gd, compound **3**, (Figure

(31) (a) Marsh, H. *Carbon*, **1987**, *25*, 49. (b) Sweatman, M. B.; Quirke, N. *Langmuir* **2001**, *17*, 5011. (c) Lozano-Castelló, D.; Cazorla-Amorós, D.; Linares-Solano, A. *Carbon* **2004**, *42*, 1233.
(32) Ehrburger-Dolle, F.; Holz, M.; Lahaye, J. *Pure Appl. Chem.* **1993**, *65*, 2223.
(33) Odler, I. *Cem. Concr. Res.* **2003**, *33*, 2049.
(34) De Jonge, H.; Mittelmeijer-Hazeleger, M. C. *Environ. Sci. Technol.* **1996**, *30*, 408.
(35) Nijkamp, M. G.; Raaymakers, J. E. M. J.; van Dillen, A. J.; de Jong, K. P. *Appl. Phys. A* **2001**, *72*, 619.
(36) Chae, H. K.; Siberio-Perez, D. Y.; Kim, J.; Go, Y.-B.; Eddaoudi, M.; Matzger, A. J.; O'Keeffe, M.; Yaghi, O. M. *Nature* **2004**, *427*, 523.
(37) Férey, G.; Mellot-Draznieks, C.; Serre, C.; Millange, F.; Dutour, J.; Surblé, S.; Margiolaki, I. *Science* **2005**, *309*, 2040.

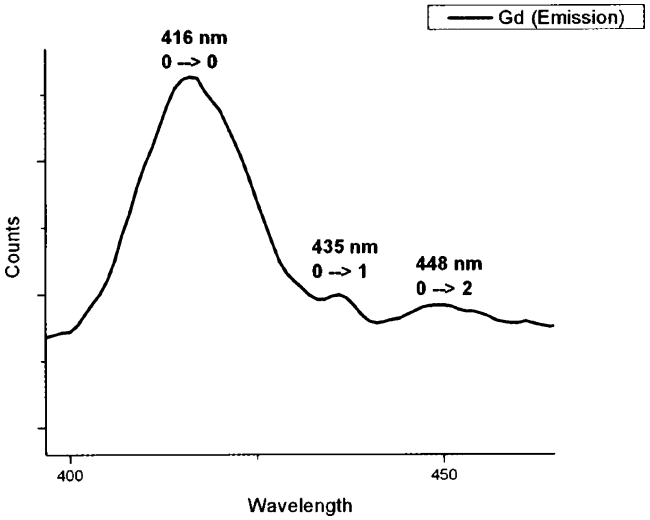

Figure 6. Phosphorescence emission spectrum for the Gd complex, **3**.

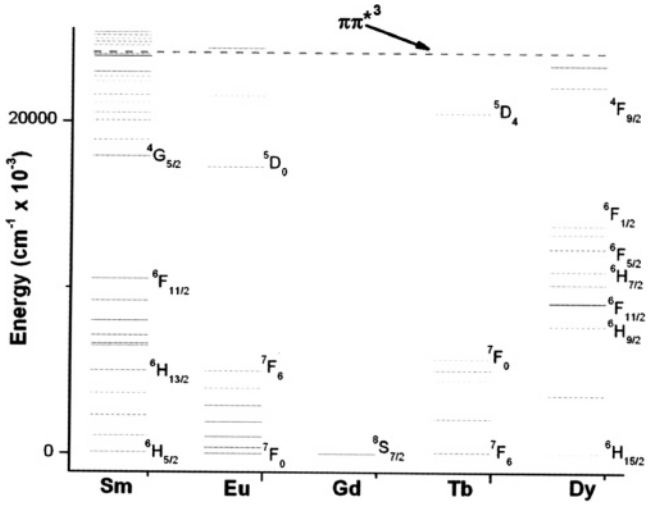

Figure 7. Energy level diagram for the lanthanides under study showing the relative energies of their emissive states versus the excited triplet state of L, indicated as the dashed horizontal line. All the Ln's but Gd are sensitized.

6). The phosphorescence from the Gd chelate is justified by the absence of any ionic resonance levels below the triplet state of the chelate. The triplet state energy levels were determined from the shortest-wavelength phosphorescence bands, which were assumed to be the 0−0 transitions.[38] As can be seen from Figure 6, three transitions, with the shortest occurring at 416 nm (24 038 cm^{-1}), are observed. Thus, as shown in Figure 7, the triplet state of L lies above the emitting states of all the metals investigated excluding Gd. As a result, L is capable of sensitizing the trivalent ions Sm, **1**; Eu, **2**; Tb, **4**; and Dy, **5**, with particularly strong emissions observed from complexes **2** and **4**.

The emission spectra obtained for the europium and terbium complexes principally arise from transitions originating at the $^5D_0$ and $^5D_4$ levels, respectively. Both metal complexes show moderate phosphorescence emission at room temperature and ambient pressure. The spectrum of the Eu complex, **2**, (Figure 8b) shows a weak band observed in the region of the $^5D_0 \rightarrow {}^7F_0$ transition. $^5D_0 \rightarrow {}^7F_1$ is the second most intense transition; it consists of a single peak slightly split into two lines. The hypersensitive transition, $^5D_0 \rightarrow {}^7F_2$, is the most intense transition and consists of an intense band with two weak shoulders at lower frequency. A less intense broad peak with a small shoulder at lower frequency is observed for the $^5D_0 \rightarrow {}^7F_3$ transition, while the $^5D \rightarrow {}^7F_4$ transition is comprised of two well-defined peaks. The room-temperature solid-state phosphorescence lifetime of the sample was determined to be 243 μs. This lifetime is shorter than that commonly observed for aromatic ligands with similar excited triplet state levels in aqueous solutions suggesting one or more nonradiative pathways are assisting in the deactivation of excited state and shortening the observed lifetimes.[39] It is known from X-ray structural data that L does not encapsulate the entire metal as only three bidentate ligands surround each metal leaving two sites ligated with water. Earlier work has established that a weak vibronic coupling between lanthanides and OH oscillators of coordinated water molecules provides a facile path for radiationless deexcitation of the metal ion.[40] Thus, the lifetimes observed are expected to be shorter due to the direct coordination of water on the lanthanide.

For europium, the splitting of the ground state levels can be readily predicted from group theory and allow for the local site symmetry of the complex to be determined.[41] When Eu^{3+} cations exist in a D_4 site symmetry, two components for the $^5D_0 \rightarrow {}^7F_1$ transition and one component of the $^5D \rightarrow {}^7F_2$ transition are expected to be observed while the $^5D_0 \rightarrow {}^7F_0$ transitions remains strongly forbidden. Figure 8b shows that while two peaks are observed for the $^5D_0 \rightarrow {}^7F_1$ transition, two weak shoulders are seen on the hypersensitive transition indicating a slight distortion from an ideal D_4 symmetry. The appearance of the $^5D_0 \rightarrow {}^7F_0$ transition is common when europium exists in a noncentrosymmetric ligand field allowing both electric-dipole and magnetic-dipole transitions to mix resulting in transitions to the "forbidden" state. The $^5D_0 \rightarrow {}^7F_3$ and $^5D_0 \rightarrow {}^7F_4$ transitions are expected to consist of two peaks each which is observed in the spectrum. Based on the experimental spectroscopic data collected, the emission spectra of complex **2** indicates a mildly distorted square antiprismatic geometry with the metal cation in a D_{4d} point symmetry. This is in excellent agreement with the X-ray structure.

The phosphorescence spectrum collected for the terbium complex **4** (Figure 8c) is impressive as all the transitions to the ground-state manifold from the emitting $^5D_4$ level are observed in moderate detail. The $^5D_4 \rightarrow {}^7F_6$ is the second largest peak observed and consists of an intense peak with a shoulder at approximately half intensity at lower frequency. As with the europium spectra, the dominant peak is the hypersensitive transition, $^5D_4 \rightarrow {}^7F_5$, which is made up of a single intense peak with a second shoulder at half the intensity. The $^5D_4 \rightarrow {}^7F_4$ and $^5D_4 \rightarrow {}^7F_2$ transitions consist of two peaks of equal intensity. Finally, there exists a weak shoulder followed by a second intense peak at lower frequency for the $^5D_4 \rightarrow {}^7F_3$ transition while the $^5D_4 \rightarrow {}^7F_1$ and $^5D_4 \rightarrow {}^7F_0$ transitions are single peaks with weak but measurable intensities. The room-temperature phosphorescence lifetime of the terbium complex was determined to be 95 μs which is reasonable considering the effect

(38) Sager, W. F.; Filipescu, N.; Serafin, S. A. *J. Phys. Chem.* **1965**, *69*, 1092.
(39) Latva, M. *J. Lumin.* **1997**, *75*, 149.
(40) Horrocks, W. D., Jr.; Sudnick, D. R. *J. Am. Chem. Soc.* **1979**, *101*, 334.
(41) Forsberg, J. H. *Coord. Chem. Rev.* **1973**, *10*, 195.

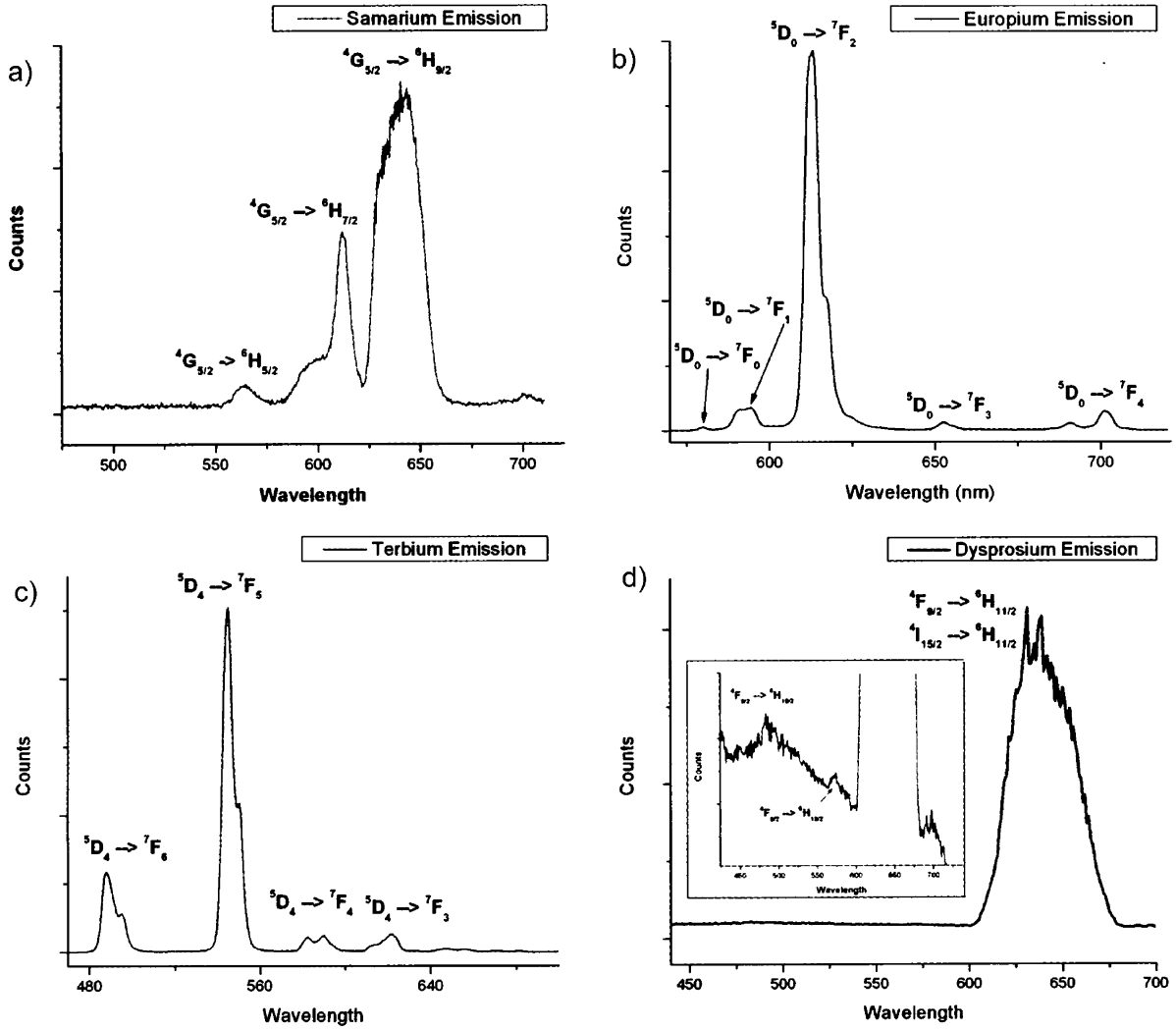

Figure 8. Luminescence spectra of compounds (a) **1**; (b) **2**; (c) **4**, and (d) **5**.

of the coordinated water molecules on quenching the excited state.

The phosphorescence spectra for the Sm and Dy complexes are significantly weaker and resolved in less detail as compared to the Eu and Tb spectra. For complex **1**, shown in Figure 8a, the $^4G_{5/2} \rightarrow {}^6H_{5/2}$ transition consists of a weak band in the yellow region. $^4G_{5/2} \rightarrow {}^6H_{7/2}$ starts as a broad shoulder then splits into a well-defined peak. The $^4G_{5/2} \rightarrow {}^6H_{9/2}$ peak is a broad and poorly resolved peak but is the most intense observed in the spectrum. A final transition, $^4G_{5/2} \rightarrow {}^6H_{11/2}$, can be observed near the beginning of the IR region and is composed of a single peak.

Upon initial investigation the Dy complex **5** (Figure 8d) appears to contain only one broad peak spanning the red region of the visible spectrum. Upon closer examination of the yellow region of the visible spectrum, two characteristic dysprosium peaks, $^4F_{9/2} \rightarrow {}^6H_{15/2}$ and $^4F_{9/2} \rightarrow {}^6H_{13/2}$, are observed albeit with very low intensity. The most intense broad peak that spans the red region of the spectrum can be described by a combination of transitions from both the lowest emitting level, $^4F_{9/2} \rightarrow {}^6H_{11/2}$, and a higher emitting hypersensitive level, $^4I_{15/2} \rightarrow {}^6H_{11/2}$, into the ground state manifold. A final weak single peak is observed and is most likely due to a combination of transitions namely $^4I_{15/2} \rightarrow {}^6H_{9/2}$ and $^4I_{15/2} \rightarrow {}^6F_{11/2}$. Lifetime measurements for both the Sm and Dy complexes are found to be 6 μs and 5 μs, respectively, based on a single-exponential fit of the data. The lack of resolution and intensity from the emission spectra from complexes **1** and **5** are due to a number of factors. First, both metals have a number of internal energy levels between the first excited state (Sm:$^4G_{5/2}$, Dy:$^4F_{9/2}$) and the ground state, (Sm:$^6H_{5/2}$, Dy:$^6H_{15/2}$). Such energy levels provide an efficient deactivation pathway of the excited state through vibrational relaxation. As noted previously, water is also directly coordinated to each metal and provides a secondary deactivation pathway. Thus while the L ligand is able to sensitize both Sm and Dy, nonradiative processes compete efficiently against photon emission.

Structural Transformations and the Nature of the Dehydrated State. Structural dynamics in MOFs are increasingly observed.[42] More detailed information on the nature of the dehydrated state was sought because it was amorphous but, at the same time, retained porosity and underwent ready rehydration to its nascent form. To relate the observed surface area to the single crystal structure, Connolly surfaces[43] were calculated for compound **2** in two scenarios, first with the noncoordinated water molecules occupying the channels removed and then with both free and coordinated water molecules removed. In the former case, a surface area of 695 m^2/gm was obtained, and in

the latter case, a surface area of 963 m^2/gm was modeled. In the Ba sulfonate solids we have prepared, we have observed typically that, upon loss of coordinated water from the Ba coordination sphere, the solid shifts structure to optimally arrange the remaining sulfonate O donor atoms about the metal ion. Thus, it was not expected that **2**, less the water molecules, would retain exactly the framework observed in the single crystal structure. More likely the framework would contract to fill the void space created. This structural shift was observed to occur, but nonetheless, the dehydrated solid still retained a high degree of porosity as evidenced by the measured surface area of 718 m^2/gm. Based on the calculated Connolly surfaces, this value is less than that expected by retention of the parent framework in an unaltered form. Qualitatively, for purposes of envisioning the degree of porosity, the extent of the structural contraction results in pores roughly equivalent to those expected for loss of only the noncoordinated water molecules in **2**.

Additional information regarding the dehydrated state was obtained by comparing spectra for the Eu complex, **2**, in its hydrated and dehydrated forms. Surprisingly, when complex **2** is dehydrated at 160 °C for 24 h, a remarkably similar emission spectrum to the original is observed suggesting only very minor rearrangement of the ligands around the metal. The most pronounced changes are in the hypersensitive, $^5D_0 \rightarrow {}^7F_2$, transition which displays only a single peak with the shoulders observed for the hydrated sample now absent. The $^5D_0 \rightarrow {}^7F_4$ transition for the dehydrated sample also undergoes a small but noticeable shift of the higher frequency peak by 3 nm to a longer wavelength. These results indicate that the coordination environment around the lanthanide undergoes mild distortions upon desolvation but preserves to a high degree the original square antiprismatic geometry. Lifetime measurements on the dehydrated sample were determined to be 319 μs. This pronounced increase from the original solvated crystals indicates that the water in both the primary and secondary coordination spheres of the metal has been predominantly removed. Subsequent measurements of the lifetimes decreased to within 10% of the original hydrated crystals under ambient conditions within 30 min, suggesting the vacant sites present in the dehydrated distorted square antiprism geometry are easily accessible to atmospheric moisture making the material very hydroscopic. Thus, while it is possible that the structural dynamics which occur upon dehydration could arise from a ligand rearrangement about the lanthanide, as is evidenced from the emission spectrum of the dehydrated sample, the L ligands remain similarly displaced about the lanthanide. The inference of this result is that the observed rearrangement must be due primarily to the groups cross-linking the building blocks. This is a reasonable expectation owing to the multiple coordination numbers and modes typically adopted by Ba centers and the ability of the SO_3 group to adopt a wide variety of coordination modes.[23a] Because of this, we have previously described the ligating properties of the sulfonate group as a "ball of Velcro."[23b]

The luminescence lifetime of **2** was examined in the presence of other solvents after heating. With MeOH, EtOH, acetone, pyridine, and nitromethane, the results indicated that, even after careful drying, the minutest amounts of water were extracted preferentially from the solvents by **2** and would coordinate to the metal centers. Hence, the changes in lifetime data were not an accurate depiction of phenomena arising from the interaction of the guests with the Ln center but, rather, the presence or absence of water.

Functional Lanthanide Metal−Organic Frameworks. The majority of research on metal−organic frameworks has concerned first-row transition metals.[44] An important reason for this is the well-studied geometrical preferences of the various ions thus facilitating network design. As a corollary, there is a relative paucity of research on lanthanide MOFs, and this is likely due to the higher coordinate and more variable nature of the Ln coordination sphere. That said, Ln centers have been explored specifically for their ability to form higher connectivity nodes in network coordination solids.[9] The pliancy of the lanthanide coordination sphere can be detrimental for porosity as it can permit structural distortion of the network which can serve to close solvated pores upon desolvation or simply allow a more facile route to a dense solid in the first place. As such, most Ln coordination frameworks that have been reported either are nonporous[15] or demonstrate only solvent sorption.[11,45] This point is exemplified by Kitagawa who has reported a Gd imidazoledicarboxylate which shows open hydrated pores.[11b] Upon dehydration, the solid shows only external surface adsorption for O_2, N_2, Ar, and CO_2 but resorbs water to give a surface area of 372.1 m^2/g. There are only a handful of lanthanide-based metal−organic frameworks which demonstrate porosity by gas sorption. These are works by Yaghi,[12] Pan,[13] and Férey[14] each employing as a ligand for the lanthanide a polycarboxylate ligand (either terephthalate, trimesate, 1,3,5-benzenetris(benzoate), or 1,4-phenylenediacetate). The use of the triply chelated Ln-building blocks with sulfonate cross-linking in this work enables the formation of a permanent porous network with the second highest surface area reported for a Ln MOF. Thus, the use of the building block approach is quite promising for further porous solids. Each network also retains the luminescent properties of the respective building block illustrating the benefits of the stepwise assembly approach.[26,27]

Conclusions. We have reported a series of isostructural lanthanide-containing metal−organic frameworks which demonstrate permanent microporosity but also incorporate predictable photophysical properties. Key to both the porosity and the fluorescence is the use of a stepwise assembly approach. The pores in **1**−**5** form due to the use of a chelated Ln coordination complex as a "clusterlike" node in a net. Dehydration resulted in a contraction, but not collapse, of the frameworks, to an amorphous material. Reversible rehydration to the nascent solid was readily observed. Furthermore, a DR surface area of 718

(42) A sampling of work related to dynamic coordination solids: (a) Uemura, K.; Kitagawa, S.; Kondo, M.; Fukui, K.; Kitaura, R.; Chang, H. C.; Mizutani, T. *Chem.−Eur. J.* **2002**, *8*, 3586. (b) Biradha, K.; Hongo, Y.; Fujita, M. *Angew. Chem., Int. Ed.* **2002**, *41*, 3395. (c) Soldatov, D. V.; Ripmeester, J. A.; Shergina, S. I.; Sokolov, I. E.; Zanina, A. S.; Gromilov, S. A.; Dyadin, Y. A. *J. Am. Chem. Soc.* **1999**, *121*, 4179. (d) Choi, H. J.; Suh, M. P. *J. Am. Chem. Soc.* **2004**, *126*, 15844. (e) Kepert, C. J.; Prior, T. J.; Rosseinsky, M. J. *J. Am. Chem. Soc.* **2000**, *122*, 5158. (f) Uemura, K.; Kitagawa, S.; Fukui, K.; Saito, K. *J. Am. Chem. Soc.* **2004**, *126*, 3817.-(g) Abrahams, B. F.; Hardie, M. J.; Hoskins, B. F.; Robson, R.; Williams, G. A. *J. Am. Chem. Soc.* **1992**, *114*, 10641. (h) Fletcher, A. J.; Thomas, K. M.; Rosseinsky, M. J. *J. Solid State Chem.* **2005**, *178*, 2491.

(43) Surfaces were calculated in Materials Studio Modeling 3.2, Accelrys Software, San Diego, CA., using a surface area of 21 $Å^2$ for CO_2.

(44) (a) Kitagawa, S.; Kitaura, R.; Noro, S. *Angew. Chem., Int. Ed.* **2004**, *43*, 2334. (b) Eddaoudi, M.; Moler, D. B.; Li, H.; Chen, B.; Reineke, T. M.; O'Keeffe, M.; Yaghi, O. M. *Acc. Chem. Res.* **2001**, *34*, 319.

(45) It should be pointed out that numerous articles have been reported where porosity is purported by the presence of solvated pores but where no evidence that the pores are sustainable or accessible is presented. For an excellent critique, see Barbour, L. J. *Chem. Commun.* **2006**, 1163.

m^2/g for the dehydrated form of compound **2** was measured by CO_2 sorption, the rigid building block enabling the formation of this porous material. Beyond serving as a structural tool, the Ln building block complex represented a predictable phosphor. Owing to this stepwise approach, the photophysical properties of the networks paralleled those of the respective building block with strong emissions observed for the Eu and Tb analogues, **2** and **4**. Luminescence spectroscopy was also employed as a diagnostic tool to gain additional insight to the nature of the amorphous microporous state. These results serve to illustrate the potential of a stepwise assembly approach to MOFs both with regard to sustaining porous structures and for purposes of incorporating predictable physical properties. From a more general perspective, the coupling of permanent porosity and luminescence in a material has interesting prospects for the development of (gas) sensor materials.[46]

(46) A mixed Ln/Mn open channel coordination polymer has recently been reported which shows luminescence emission intensity dependent on metal ions added to the solution. Zhao, B.; Chen, X.-Y.; Cheng, P.; Liao, D.-Z.; Yan, S.-P.; Jiang, Z.-H. *J. Am. Chem. Soc.* **2004**, *126*, 15394.

Acknowledgment. We thank Dr. Frank van Veggel of the University of Victoria for allowing some of the luminescence measurements to be performed in his laboratory. We thank Quantachrome Instruments for performing the initial CO_2 and N_2 sorption analyses. We also acknowledge support from the Natural Sciences and Engineering Research Council (NSERC) of Canada for Discovery Grants to D.T.C. and G.K.H.S. and the Canadian Institute for Photonics Innovation (CIPI) for a grant to D.T.C.

Supporting Information Available: CIF files for **1**−**5**, details of complete characterization of **1**−**5**. This material is available free of charge via the Internet at http://pubs.acs.org.

JA060666E